Journal of Materials Physics and Chemistry, 2026, Vol. 14, No. 1, 22-31
Available online at http://pubs.sciepub.com/jmpc/14/1/3
Published by Science and Education Publishing
DOI:10.12691/jmpc-14-1-3

Low-KOH Co-carbonization of Sugarcane Bagasse and Coconut Shell Blends: Effects of Blending Ratio on Activated Carbon Properties

Francis Ngoye[1,2,*], Ornellia Nargess Ozenga[1], Pradel Tonda-Mikiela[1], Rodrigue Safou Tchiama[2], Charly Mve Mfoumou[1]

[1]Laboratoire de Chimie des Milieux et des Matériaux Inorganiques (LC2MI), URCHI/ Université des Sciences et Techniques de Masuku (USTM), BP: 943 Franceville-Gabon
[2]Laboratoire de Recherche et de Valorisation du Matériau Bois (LaReVa-Bois). Ecole Normale Supérieure d'Enseignement Technique (ENSET), BP: 3989, Libreville-Gabon
*Corresponding author: ngoyefrancis@yahoo.fr

Received July 17, 2026; Revised August 19, 2026; Accepted August 26, 2026

Abstract Co-carbonizing agricultural residues represents an efficient strategy to tailor activated carbon properties while reducing chemical activating agents. In this work, activated carbons (ACs) were prepared by blending sugarcane bagasse and coconut shell at different mass ratios, followed by pre-carbonization at 350 °C, KOH impregnation at a low mass ratio of 0.1:1 (*w/w*), and activation at 600°C. Characterization via Boehm titration, pH_{pzc}, iodine number, and methylene blue number revealed that the precursor ratio influences both structural and chemical properties. Specifically, the bagasse-rich blend (CA-B80) showed the highest estimated specific surface area (576 $m^2.g^{-1}$) and micropore volume (0.382 $cm^3.g^{-1}$) among the samples, pointing to a positive textural effect during co-carbonization. Conversely, the coconut-rich blend (CA-B20) presented the highest concentration of carboxylic groups (1.31 $mmol.g^{-1}$), suggesting a distinct trend in surface chemistry enhancement. In batch adsorption tests, CA-B50 and CA-B20 achieved methylene blue uptake capacities of 492 and 477 $mg.g^{-1}$, respectively, outperforming single-precursor analogues. These findings demonstrate that co-carbonization provides a sustainable and cost-effective route to valorize tropical biomass wastes with minimal chemical demand.

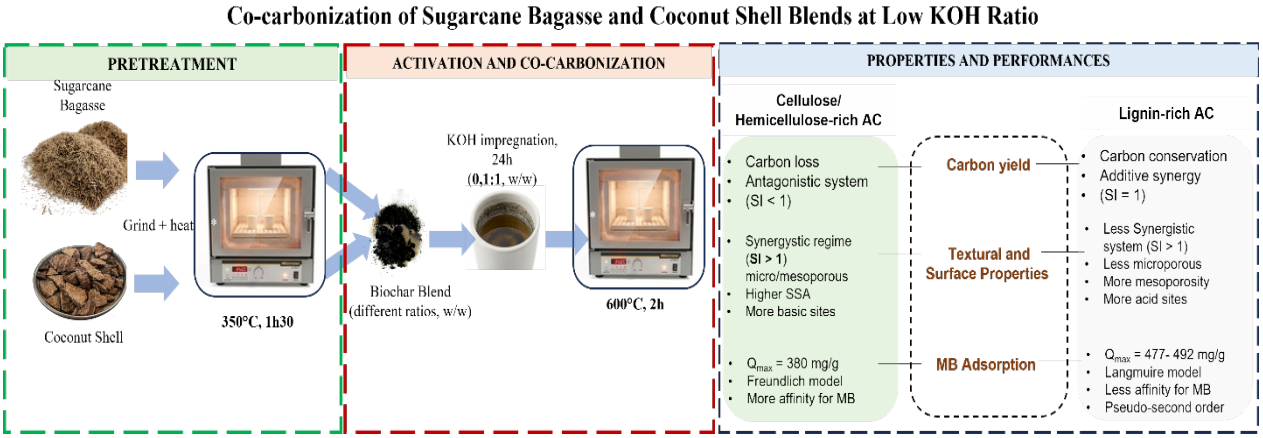

Keywords: *Activated carbons, Sugarcane bagasse, Coconut Shell, Co-Carbonization, Low KOH Activation, Methylene blue adsorption*

Cite This Article: Francis Ngoye, Ornellia Nargess Ozenga, Pradel Tonda-Mikiela, Rodrigue Safou Tchiama, and Charly Mve Mfoumou, "Low-KOH Co-carbonization of Sugarcane Bagasse and Coconut Shell Blends: Effects of Blending Ratio on Activated Carbon Properties." *Journal of Materials Physics and Chemistry*, vol. 14, no. 1 (2026): 22-31. doi: 10.12691/jmpc-14-1-3.

1. Introduction

The conversion of agricultural and industrial residues into porous carbon materials has attracted considerable attention as a sustainable approach to both waste valorization and environmental remediation. Among these materials, biochar and activated carbon (AC) have been widely investigated for applications including wastewater treatment, gas purification, energy storage, and CO_2 capture [1,2,3]. Sugarcane bagasse (SB) and coconut shell (CS) are among the most widely studied lignocellulosic precursors because of their abundance, low cost, and complementary structural characteristics. Nevertheless, most reported activated carbons derived from these feedstocks have been produced from a single biomass precursor [4,5,6].

To improve pore development and material performance, increasing attention has been directed toward co-carbonization, in which two complementary feedstocks are thermochemically converted together. This approach has been reported to promote a more balanced pore network [7], improve mechanical stability [8], and generate a self-activation effect through mutual gas-phase interactions during pyrolysis [9]. Most published studies, however, have focused on blends of biomass with coal [10,11], sewage sludge [12,13], livestock manure and slurries or algae [14], often targeting the production of energy-related products such as bio-oils, combustible gases, or carbon electrodes for supercapacitor applications [3]. In contrast, the preparation of ACs from blends of two lignocellulosic biomasses, particularly SB and CS, for adsorption-based water treatment remains sparsely documented in the literature surveyed, highlighting an opportunity for further investigation.

Another common feature of the reported co-activation processes is the use of relatively high chemical impregnation ratios, typically ranging from 1:1 to 5:1 (Activating agent/biomass, w/w) [15,16,17], to enhance pore development. Although such conditions are commonly employed to maximize porosity, they are also likely to increase reagent consumption, production costs, and the environmental footprint of the process, which may limit their practical applicability, particularly in resource-constrained settings. The literature surveyed did not reveal studies describing the co-carbonization of an SB/CS blend in a single crucible followed by chemical activation using a KOH impregnation ratio as low as 0.1:1. This approach could therefore represent a more sustainable and economically attractive alternative by reducing chemical consumption while maintaining the potential to produce effective activated carbons.

Against this background, this study investigates the co-carbonization of sugarcane bagasse and coconut shell blends in a single crucible, followed by chemical activation using a low KOH-to-biomass mass ratio (0.1:1). It is hypothesized that combining these complementary lignocellulosic feedstocks under mild activation conditions can promote the development of activated carbons with physicochemical properties suitable for adsorption while reducing chemical consumption. To examine this hypothesis, the prepared materials were characterized using widely established methods requiring limited instrumentation, including Boehm titration [18,19,20], ASTM D4607 [21], the CEFIC reference method [22], and the protocol proposed by Nunes *et al.* [23]. Adsorption performance was subsequently evaluated using methylene blue (MB) as a model pollutant, and the equilibrium data were analyzed using the Langmuir and Freundlich isotherm models. Beyond assessing the adsorption potential of the prepared materials, this work aims to explore a simpler and potentially more resource-efficient route for producing activated carbons from locally available lignocellulosic residues.

2. Materials and Methods

The biomass precursors used in this work were sourced locally in the Haut-Ogooué province of Gabon. CS were purchased from the municipal market in Franceville, while SB was collected from the company "Les *Sucreries du Gabon"*.

2.1. Activated Carbons Preparation

The samples were washed separately with a large amount of water to remove surface impurities, then air-dried for one week, followed by oven drying at 110°C for 24h. The samples were then ground separately and pre-calcined at 350°C for 1h30 using a NABERTHERM muffle furnace. After pre-carbonization, the materials were ground again and sieved using a mesh size of less than 0.1mm. The sieved powders were used to prepare two sets of samples. The first set was consisted of raw materials (SB and CS) used separately. The second set consisted of precursors SB and CS mixtures at different proportions (80/20, 50/50 and 20/80). The materials were then impregnated for 24h in potassium hydroxide solution (KOH, 1M), using a low KOH-to-biomass mass ratio of 0.1:1 (*w/w*). After impregnation, the mixture was filtered and the solid was dried in an oven at 110°C for 24h, followed by carbonization at 600 °C for 2h. The obtained ACs were washed with 50 ml of hydrochloric acid solution (HCl, 1M) and then thoroughly rinsed with hot distilled water until neutral pH (≈ 6.5 - 7.5) was reached, in order to remove oxides formed during carbonization and any residual activating agent. The ACs were designated as CA-B, CA-C, CA-B20, CA-B50 and CA-B80, corresponding respectively to ACs derived from SB, CS, SB and CS blends (20/80, 50/50 and 80/20).

2.2. Determination of Carbonization Yields

The pre-carbonization yield (Y_{pc}) and carbonization yield (Y_c) were quantitatively evaluated in the AC production process. These yields were calculated from the masses measured at different stages of the process [24,25] and constitute essential indicators for characterizing the thermochemical conversion of our raw materials. To evaluate the potential advantage of co-carbonization compared to the separate carbonization of the two materials, a theoretical yield (Y_{th}) was calculated assuming the additivity of the individual contributions of each raw material [24]. Thus, the tree yields were calculated using the following equations:

$$Y_{pc} = \frac{m_{pc}}{m_i} \times 100 \quad (1)$$

$$Y_c = \frac{m_c}{m_i} \times 100 \quad (2)$$

$$Y_{th} = w_1 Y_1 + w_2 Y_2 \quad (3)$$

where:

m_i, m_{pc} and m_c are respectively the initial biomass mass (g), the mass (g) after pre-carbonization and the mass (g) of AC obtained after carbonization. Y_{pc}, Y_c and Y_{th} are respectively the pre-carbonization yield (%), the carbonization yield (%) and theoretical yield (%) of the blend. w_1 and w_2 are the mass fractions of the two biomasses in the blend. Y_1 and Y_2 are the carbonization yields of the two biomasses when processed separately.

2.3. Determination of Methylene Blue Number, Iodine Number and Structural Properties

The methylene blue number (MBN) and iodine number (IN) were determined according to the method of the European Chemical Industry Council (CEFIC, 1986) [22] and the ASTM D4607-94 standard [21], respectively. These two methods were adapted and previously described in earlier works developed within our laboratory [26]. Thus, the MBN is calculated using the following equation:

$$MBN = \frac{(C_0 - C_r) \times V}{m_{CA}} \quad (4)$$

where MBN is the methylene blue number ($mg.g^{-1}$), C_0 is the initial concentration ($mol.L^{-1}$) of MB, C_r is the residual concentration ($mol.L^{-1}$) of MB, V is the volume (L) of MB solution and m_{CA} is the mass (g) of AC.

The iodine number was calculated using the following equation:

$$IN = \frac{\left(C_{I_2} \times 126.93 \times V_{I2}\right)}{m_{CA}} - \frac{DF \times \left(126.93 \times C_{NaS_2O_3}\right) \times V_{NaS_2O_3}}{m_{CA}} \quad (5)$$

where

IN is iodine number ($mg.g^{-1}$), C_{I_2} is the concentration ($mol.L^{-1}$) of iodine (I_2) solution, V_{I_2} is the volume (L) of I_2, DF is the dilution factor ($DF = \frac{V_{I2} + V_{HCl}}{V_{filtrat}}$), $C_{NaS_2O_3}$ is the concentration ($mol.L^{-1}$) of sodium thiosulfate solution and $V_{NaS_2O_3}$ is the volume (L) of sodium thiosulfate solution.

The structural properties of ACs were estimated using empirical correlation established by Nunes *et al.* [23], which relate MBN and IN to the estimated specific surface area ($S_{est.}$) and pore characteristics. The following equations were applied:

$$S_{est.} = 2.28 \times 10^2 - 1.01 \times 10^{-1} \times MBN + 3 \times 10^{-1} \times IN + 1.05 \times 10^{-4} \times MBN^2 + 2 \times 10^{-4} \times IN^2 + 9.38 \times 10^{-4} \times MNB.IN \quad (6)$$

$$V_T = 1.37 \times 10^{-1} + 1.90 \times 10^{-3} \times MBN + 1.00 \times 10^{-4} \times IN \quad (7)$$

$$V_{micro} = 5.60 \times 10^{-2} - 1.00 \times 10^{-3} \times MBN + 1.55 \times 10^{-4} \times IN + 7.00 \times 10^{-6} \times MBN^2 + 1.00 \times 10^{-7} \times IN^2 - 1.18 \times 10^{-7} \times MBN.IN \quad (8)$$

$$V_{meso} = V_T - V_{micro} \quad (9)$$

where:

S_{est} is the estimated specific surface area ($m^2.g^{-1}$), V_T is total pore volume ($cm^3.g^{-1}$), V_{micro} is the micropore volume ($cm^3.g^{-1}$), V_{meso} is mesopore volume, MBN is the methylene blue number ($mg.g^{-1}$) and IN is the iodine number ($mg.g^{-1}$). According to the authors, the estimated values align closely experimental BET measurements, yielding a relative error of less than 15%.

2.4. Determination of Surface Functional Groups

The surface functional groups of the ACs were determined using the Boehm method [18,19,20], which is based on the selective neutralization of acidic and basic functions present on the material surface. This approach allows the quantification of different oxygenated functional groups, including carboxylic, lactonic, and phenolic groups, as well as basic sites. A 100 mg sample of AC, was immersed for 24h in 25 mL of basic solutions with increasing strength, namely sodium bicarbonate ($NaHCO_3$, 0,1M), sodium carbonate (Na_2CO_3, 0,05M) and sodium hydroxide (NaOH, 0,1M), in order to neutralize carboxylic group, carboxylic plus lactonic groups, and all acidic functions, respectively. After filtration, the solutions were analyzed by acid-base titration to determine the amount of reagent consumed. The hydrochloric acid solution (HCl, 0,1M) was used to quantify the basic surface sites. The concentration of the different surface functional groups was calculated using the following equation:

$$n = \frac{(V_b - V_e) \times C \times 1000}{m_{CA}} \quad (10)$$

where

n is the amount ($mmol.g^{-1}$) of surface functional group, V_b is the volume (L) of the blank, V_e is the volume (L) of the sample, C is the concentration ($mol \cdot L^{-1}$) of the titrant solution and m_{CA} (g) is the mass of the AC.

2.5. Determination of Point of Zero Charge

The point of zero charge (pH_{pzc}) of the ACs was determined using the pH drift method described by Kifuani *et al.* [27]. Briefly, 40 mg of the AC was added to a series of six beakers containing 20 mL of potassium chloride (KCl, 0.01 M) solution. The initial pH (pH_i) of the solutions was adjusted across a range from 2 to 12using HCl (0.1 M) or NaOH (0.1 M). The suspensions were stirred for 24h to reach equilibrium. After settling, the final pH (pH_f) was measured. The pH_{pzc} was graphically determined as the abscissa of the intersection point of the experimental curve with the diagonal line ($pH_f = pH_i$).

2.6. Determination of Synergy Index

The synergistic effect during the co-pyrolysis of SB and CS blends were evaluated based on the textural properties of the produced ACs, namely, the specific surface area (SSA) and pore volumes (micropore, mesopore and total volume). The Synergistic Index (SI) was calculated by comparing the experimental values obtained for the blends with the theoretical values estimated from linear combination of the individual precursors. The SI is defined as [28]:

$$SI = \frac{X_{\exp}}{X_{th}} \quad (11)$$

$X_{\exp}$ is the experimental value of a given parameter (SSA, pore volume, functional group) of ACs obtained from the mixture, X_{th} is the theoretical value calculated using the rule of mixtures:

$$X_{th} = w_1 X_1 + w_2 X_2 \quad (12)$$

where

w_1 and w_2 represent the mass fraction of bagasse and coconut shells, respectively, in the initial mixture, while X_1 and X_2 correspond to the textural properties of ACs derived from each precursor individually.

2.7. Evaluation of the Adsorptive performance of Activated Carbons

Adsorption tests were carried out in a batch mode at room temperature and at pH ≈ 6.7, using MB as the model pollutant.

For the kinetic study, an initial concentration of C_0 =120 mg.L^{-1} was used. A mass of 25 mg of ACs was contacted with 100 mL of solution. The mixture was stirred for contact times ranging from 5 to 120 minutes in order to monitor the adsorption kinetic. After each contact time, the suspensions were filtered and the residual MB concentration was determined using UV-Visible spectrophotometer (Thermo Electron Corporation Biomate 5).

For the adsorption isotherm studies, MB solution with initial concentrations ranging from 60 to 120 mg.L^{-1} were treated under de same conditions as those employed in the kinetic study. The mixtures were agitated for 2h to ensure that the equilibrium was reached. The equilibrium adsorption capacity q_e (mg.g^{-1}) was calculated using the mass balance equation:

$$q_e = \frac{(C_0 - C_e)V}{m} \quad (13)$$

where C_0 and C_e (mg.L^{-1}) are the initial and equilibrium concentrations, V (L) is the solution volume, and m (g) is the mass of AC.

The adsorption isotherm data were analyzed using the Langmuir and Freundlich models. The non-linear Langmuir model is expressed as:

$$q_e = \frac{Q_{\max} K_L C_e}{(1 + K_L C_e)} \quad (14)$$

where Q_{max} (mg.g^{-1}) is the maximum adsorption capacity and K_L (L/mg) is the Langmuir constant.

The Freundlich model is given by:

$$q_e = K_F C_e^{\frac{1}{n}} \quad (15)$$

where K_F is the Freundlich model and n is the heterogeneity factor.

The model parameter fitting was performed using non-linear regression with the excel solver tool, allowing simultaneous estimation of model constant and evaluation of fitting quality.

The intraparticle diffusion model proposed by Weber and Morris was also applied to further investigate the possible contribution of pore diffusion to the adsorption kinetics. The intraparticle diffusion rate constant (k_{id}) and the intercept (C) were determined from the corresponding plots, with C providing an indication of the boundary-layer effect.

3. Results and Discussion

3.1. Carbonization Yields

Table 1 presents the carbonization yields (Y) and the synergy index (SI) of ACs. The results showed a decrease in yield between Y_{pc} and Y_c. Y_{pc} values ranged between 30.6 and 39.9 %, whereas Y_c varied from 21.1 to 27.3%. The lowest losses in yield between Y_{pc} and Y_c were observed for CA-C (6.6%), CA-B (6.3%) and CA-B20 (6.4%), while the highest losses were obtained for CA-B80 (9.5%) and CA-B50 (8.4%). The comparison between Y_c and Y_{th} revealed a non-linear behavior in the co-carbonization process [24,29]. For CA-B80 and CA-B50, experimental yields were lower than theoretical prediction, indicating a negative deviation from the additive rule [29]. In contrast, CA-B20 exhibited nearly identical values between Y_c and Y_{th}, suggesting a transition to ideal mixing behavior. The SI describing deviations from additive behavior during co-carbonization of bagasse and coconut shells showed values below unity for CA-B50 (0.92) and CA-B80 (0.86), indicating antagonistic interactions [29,30], while value approaching unity was observed for CA-B20 (1.01), suggesting progressive stabilization of carbon yield with increasing coconut content.

Table 1. Carbonization yields and synergy index

Samples	Y_{pc}(%)	Y_c (%)	Y_{th} (%)	**SI**
CA-B	29.9	23.6	-	-
CA-C	33.9	27.3	-	-
CA-B80	30.6	21.1	24.3	0.86
CA-B50	31.8	23.4	25.5	0.92
CA-B20	33.1	26.7	26.5	1.01

Y_{pc}: Pre-carbonization, **Y_c**: final carbonization, **Y_{th}**: theoretical yields, **SI**: Synergy Index

Overall, it was observed that for ACs prepared by co-carbonization, the mass loss increased with increasing

bagasse content. Indeed, carbonization generally leads to mass loss due to the removal of water; volatile compounds, and the decomposition of thermolabile compounds [31]. The variation in yield observed among the samples may be explained by the difference of their chemical composition. Bagasse is rich in cellulose and hemicellulose, which is readily decomposed into volatiles products at low temperatures resulting in antagonistic behavior and lower carbon yields, whereas increasing coconut shells content enhances aromatic structure development and carbon stabilization, progressively shifting the system toward additive or slightly synergistic system behavior. Coconut likely acts as a structural carbonization matrix due to the lignin which is known as thermally stable [32]

However, the carbonization yields (21.1-26.7%) are close to or higher than those reported in the literature [33] for the ACs produced at moderate temperature. To select the best adsorbent, it is necessary to compare the yields with the textural and the physicochemical properties [34].

3.2. Textural Properties and Effect of Biomass Blending

The textural properties (Table 2) of the prepared ACs were evaluated and compared using iodine and MB adsorption tests. These two compounds, which reflect the adsorption capacity toward small molecules associated with microporosity and larger molecules related to more accessible pores [23,35], respectively, were used as probe molecules to estimate the pore distribution based on the empirical correlation established by Nunes *et al. [23]*. The IN and MBN measured as well as the pore parameters are reported in Table 2. The results showed a significant influence of the bagasse/coconut shells ratio on IN and MBN.

CA-C exhibited the lowest IN value (33.70 $mg.g^{-1}$), indicating a limited development of accessible microporosity under the applied activation conditions. Although coconut shell is generally considered a suitable precursor for producing highly microporous activated carbons, the low KOH-to-biomass ratio used in this study (0.1:1) may have been insufficient to extensively promote pore development within its dense carbon structure. Similar observations have been reported for coconut shell-derived carbons prepared under mild activation conditions, where the resulting materials exhibited limited microporosity or a greater contribution of mesopores to the pore network [36,37].

In contrast, CA-B80 showed the highest iodine number (391.75 $mg.g^{-1}$), exceeding those of the individual precursors, suggesting a beneficial effect of combining bagasse and coconut shell during co-carbonization [38]. The intermediate IN values obtained for CA-B50 and CA-B20 indicate that decreasing the proportion of bagasse gradually reduced the development of accessible micropores. The methylene blue number (MBN) followed a similar trend, with values ranging from 196.08 to 277.78 $mg.g^{-1}$ and the highest adsorption capacity observed for CA-B80, reflecting improved accessibility of larger pores. However, the differences between samples were less pronounced than those observed for IN, suggesting that biomass blending mainly influenced micropore development rather than mesopore accessibility [39]. The estimated specific surface area ($S_{est.}$), calculated from the iodine number according to the correlation proposed by Nunes et *al.* [23], followed the same trend as the adsorption indices. CA-B80 exhibited the highest S_{est} (575.75 $m^2.g^{-1}$), together with the highest micropore volume (0.382 $cm^3.g^{-1}$) and total pore volume (0.704 $cm^3.g^{-1}$), confirming the greater development of its porous structure.

These results suggest that the combination of SB and CS during co-carbonization promoted the formation of a more accessible pore network, likely due to complementary contributions from both precursors during carbonization and activation [40]. The pre-carbonization step followed by KOH activation may also have contributed to a more controlled development of the carbon structure, as reported for two-stage pyrolysis approaches [30]. The differences in mesopore volume among the samples were relatively limited, ranging from 0.322 to 0.380 $cm^3.g^{-1}$. Therefore, the superior adsorption performance of CA-B80 appears to be mainly related to enhanced micropore development rather than significant changes in mesoporosity [41,42].

Table 2. Textural properties of activated carbons

Samples	IN ($mg.g^{-1}$)	MBN ($mg.g^{-1}$)	$S_{est.}$ ($m^2.g^{-1}$)	V_{micro} ($cm^3.g^{-1}$)	V_{meso} ($cm^3.g^{-1}$)	V_t ($cm^3.g^{-1}$)
CA-B	261.44	196.08	430.80	0.170	0.365	0.536
CA-C	33.70	204.08	242.80	0.148	0.380	0.528
CA-B20	283.19	208.33	452.80	0.196	0.365	0.561
CA-B50	250.15	212.77	423.80	0.199	0.367	0.566
CA-B80	391.75	277.78	575.90	0.382	0.322	0.704

IN: Iodine Number, **MBN**: Methylene Blue Number, $\mathbf{S_{est}}$: Estimated Specific Surface Area, $\mathbf{V_{micro}}$: micropore volume, $\mathbf{V_{meso}}$: mesopore volume, $\mathbf{V_t}$: total pore volume The synergistic effect of biomass blending was further evaluated using the synergy index (SI) (Figure 1).

Figure 1 shows that the SI was influenced by the blending ratio. The highest synergistic effect was observed for the micropore volume of the bagasse-rich blend (CA-B80), with a SI of 2.30. The estimated specific surface area also showed a positive, although less pronounced, synergistic effect. In contrast, the mesopore volume remained close to the additive behaviour (SI ≈ 1), indicating that co-carbonization mainly promoted micropore formation rather than mesopore development. This behaviour can be explained by the complementary thermal degradation of SB and CS during pre-carbonization, which likely produced a carbon matrix with a greater number of reactive sites. Under the same activation conditions, KOH was therefore able to react more efficiently with this matrix, favoring the development of micropores during carbonization at 600°C,

in agreement with previous studies on two-step activation processes [25,40]. The relatively lower carbonization yield of CA-B80 further supports this interpretation, as micropore formation generally occurs through partial gasification of the carbon matrix during chemical activation [43]. Consequently, the increase in the estimated specific surface area is mainly associated with enhanced micropore development, while mesoporosity remains only slightly affected by biomass blending.

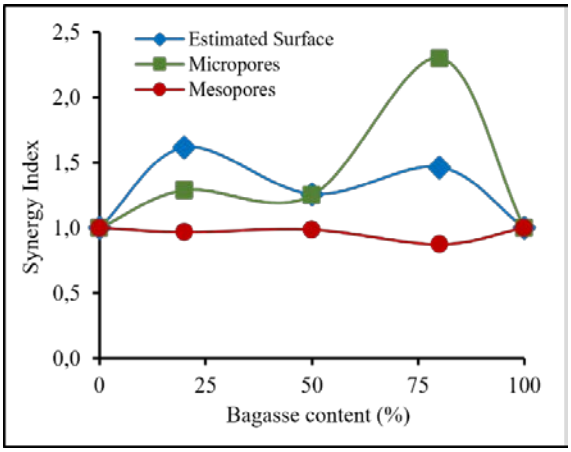

Figure 1. Synergistic effect on textural properties

3.3. Surface Chemistry and Interfacial Properties

Table 3 presents the surface chemical properties of ACs obtained from individual precursors and their mixtures, impregnated with a very low mass ratio of activating agent to biomasses (0.1:1, *w/w*) and carbonized at 600°C. The analysis focused on surface functional groups, total acidity, and the pH_{pzc} as a function of sample composition. The results showed high total acidity (1.83-3.63 $mmol.g^{-1}$), associated with relatively low basicity (0.91-1.36 $mmol.g^{-1}$).

Table 3. Surface functional groups of activated carbons

Samples	Content ($mmol.g^{-1}$)					
	Carboxylic	Lactonic	Phenolic	Acidity	Basicity	pH_{pzc}
CA-CC	0.81	0.50	0.50	1.81	1.02	6.45
CA-B	0.94	0.63	2.06	3.63	0.94	6.60
CA-B20	1.31	0.63	1.06	3.00	0.97	6.90
CA-B50	1.13	0.25	0.69	2.06	0.91	6.80
CA-B80	1.13	0.19	1.38	2.69	1.36	6.70

Although KOH is generally known to produce basic carbons, this behavior was not observed in the present study, suggesting that under these experimental conditions it mainly acted as a carbon network restructuring and pore-developing agent rather than a direct source of basic surface functionalities. The prior pre-carbonization of the biomasses also limited further changes in surface chemistry during activation. However, these absolute values do not fully reflect the interactions occurring between the different precursors in the mixed samples. A more appropriate interpretation can be obtained by considering the synergistic effects (Figure 2) of each surface functionality relative to their expected additive behavior. This approach helps to distinguish simple compositional effects from true interaction induced changes in surface chemistry.

The experimental data in Figure 2 showed that the SI of the surface functional groups vary nonlinearly with the bagasse fraction during KOH activation followed by carbonization at 600°C [41]. At low bagasse content (20%), a synergistic effect was observed for acidic surface sites, particularly carboxylic groups (SI ≈ 1.58) and phenolic groups (SI ≈ 1.35). This, suggests that the moderate addition of bagasse promotes the formation or exposure of oxygen containing acidic groups during activation [41].

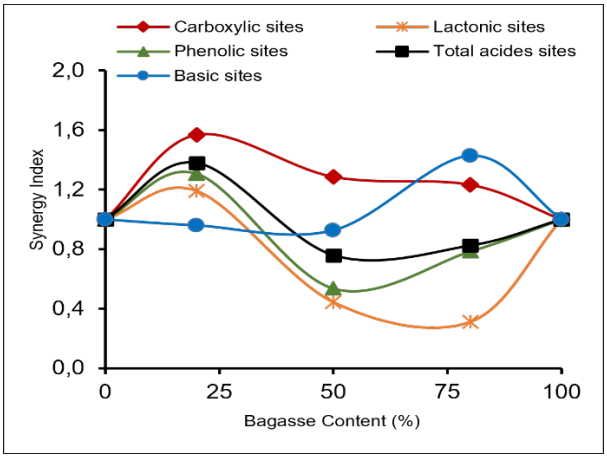

Figure 2. Synergistic effect on functional groups

In contrast, lactonic groups exhibit a strong antisynergistic behavior, descreasing to SI ≈ 0.28 at around 80% bagasse content. The decrease in lactonic content observed in mixtures enriched in cellulose and hemicellulose-derived precursors (bagasse) can be attributed to their lower propensity to generate stable oxygen-containing aromatic intermediates during carbonization. These polysaccharide-rich components undergo extensive devolatilization [42], leading to oxygen loss and the formation of a less functionalized carbon matrix, which in turn limits lactone formation. Under the same conditions, basic sites increase significantly, reaching SI ≈1.43. This behavior can be explained by relative increase of basic sites in condensed aromatic domain, which enhances π-electron density and consequently increases surface basicity through the development of Lewis- type basic sites. From an applications perspective, low bagasse proportion favor acidic sites that may be beneficial for acid catalysis or selective adsorption, whereas, high bagasse proportion promotes a more basic surface character [44].

The pH_{pzc} values do not show a direct linear relationship with either total acidity or basicity [45], indicating that surface charge behavior is not governed solely by the absolute concentration of acidic and basic sites. Instead, the observed variations reflect the combined effect of synergistic interactions between precursors [41], witch a redistribution of oxygen-containing functional groups [40] and a modification of electronic character of the carbon surface.

In particular, the highest pH_{pzc} value (6.90 for CA-B20) suggests that intermediate compositions promote a more pronounced structural reorganization, leading to a surface where acidic functionalities are less electrochemically effective and partially compensates by the formation of less proton-affine aromatic domains [44]. This behavior contrast with CA-B (pH_{pzc} = 6.60), despite its higher acidity (3.63 mmol/g), confirming that acidity alone does not dictate surface charge properties.

At higher proportion of bagasse, the pH_{pzc} slightly decrease to 6.80 (CA-B50) and 6.70 (CA-B80), respectively. This trend coincides with an increase in basic sites for CA-B80 (1.36 mmol/g), suggesting that the development of π-electron-rich domains partially compensates for surface acidity [44] and moderates the overall surface charge behavior. In comparison, CA-C exhibits the lowest pH_{pzc} value (6.45), consistent with its lower degree of structural reorganization.

3.4. Adsorptive Performances

Figure 3 shows the adsorption kinetics of MB as function of time for an initial concentration of 120 $mg.L^{-1}$. The kinetic curves show very fast adsorption during the first few minutes (0-8 min), followed by a gradual slowdown until a plateau is reached after 10 min, indicating that equilibrium has been established [46]. This behavior suggests that the molecules first attach quickly to the most accessible sites, and then diffuse more slowly into the internal pores of the ACs.

The adsorption equilibria were conducted by plotting the evolution of the equilibrium adsorption capacity (Q_e) as function of residual concentration (C_e) of MB (Figure 4) obtained for initial concentrations from 12 to 120 $mg.L^{-1}$. For all the samples, the experimental data describe L-class curves (according to Giles'classification) [47], characterized by a sharp initial slop (notably for CA-B80) followed by a gradual leveling off. However, within the studied concentration range, the experimental isotherms show only a slight saturation plateau, with the capacity Q_e continuing to increase moderately at the highest concentrations. Mathematical fitting of these profiles was performed using non-linear regression, allowing for a comparison of the suitability of the Langmuir and Freundlich models [48].

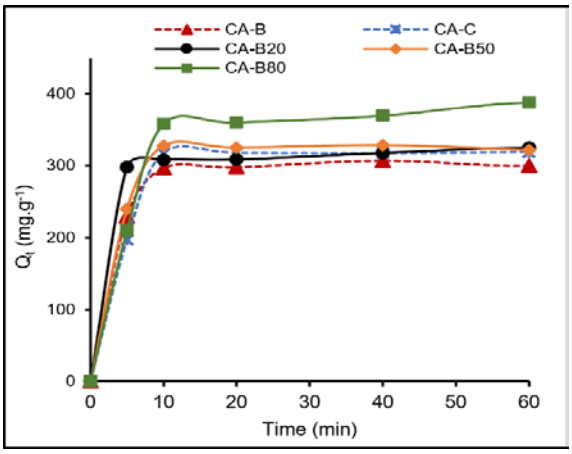

Figure 3. Adsorption kinetics of MB at an initial concentration of 120 $mg{\cdot}L^{-1}$

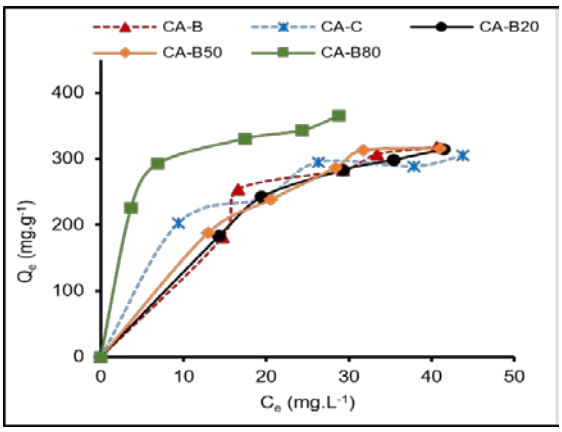

Figure 4. Adsorption isotherms of MB

The results of Table 4 show that MB adsorption is favorable for all the samples. The R_L values, ranging from 0.0174 to 0.1475, are all below 1, confirming the favorable nature of the process [48]. Likewise, the *n* values obtained from Freundlich model are greater than 1 for all ACs, indicating a good affinity between MB and ACs surfaces [48].

The kinetic analysis also shows that the pseudo-second-order model fits the experimental behavior very well for all ACs, with R^2 values ranging from 0.9985 to 0.9991. However, a good fit to the pseudo-second-order model alone does not establish a chemisorption mechanism. The Weber–Morris analysis provided further insight into the mass-transfer processes involved. The relatively low R^2 values (0.479–0.564) and the non-zero intercepts (C = 74.17–153.32 $mg.g^{-1}$) indicate that intraparticle diffusion alone does not control the overall adsorption kinetics. Instead, the adsorption process likely involves a combination of boundary-layer mass transfer, pore diffusion, and adsorbate–surface interactions [46]. Interestingly, CA-B50 exhibited the highest k_{id} value (42.10 mg g^{-1} $min^{-0.5}$), together with a relatively low C value (74.55 mg g^{-1}), indicating a comparatively higher apparent intraparticle diffusion rate. This behavior was observed for the sample that also exhibited the highest methylene blue adsorption capacity (492 mg g^{-1}), although the adsorption performance cannot be attributed to intraparticle diffusion alone.

CA-B, CA-C, CA-B20, and CA-B50 are better described by the Langmuir model, which indicates a dominant tendency toward monolayer adsorption on relatively homogeneous sites. In contrast, CA-B80 shows a better fit to the Freundlich model, reflecting a more heterogeneous surface and a wider distribution of active sites [48,49]. This interpretation is consistent with its high K_F value (219.60), witch points to a strong overall affinity for MB.

Although the CA-B80 curve shows a higher experimental capacity (Q_{exp} = 364 $mg.g^{-1}$) than the other samples within the studied concentrations range, the Langmuir model extrapolates a lower Q_{max} (380 $mg.g^{-1}$). This is due to its high affinity (K_L = 0,4699), which quickly approaches saturation. In contrast, other samples have a lower affinity (0,0481 - 0.1378) but possess a much larger pool of active sites and mesoporosity, suggesting that the curves might cross at higher concentrations beyong the experimental range. In terms of maximum capacity, CA-B50 exhibit the highest value, with Q_{max} =

492 mg.g^{-1}, followed by CA-B20 (477 mg.g^{-1}) and CA-B (462 mg.g^{-1}). This result indicates that a highly developed microporosity is not necessary the most decisive advantage for a relatively large molecule such as MB [50,51]. In this AC, a better balance between micro- and mesoporosity appears more favorable, as it improves access to the internal sites.

CA-B50 therefore emerges as the best-performing material in therms of Q_{max}. While CA-B80 stands out mainly for its kinetic consistency and strong affinity. To further assess the relevance of the obtained activated carbons, their preparation conditions and adsorption-related properties were compared with previously reported biomass-derived activated carbons (Table 5).

Table 5 provides a comparison between the activated carbons prepared in this study and previously reported biomass-derived activated carbons. In general, chemical activation leads to a more developed porous structure than physical activation; however, the highest surface areas reported in the literature are often obtained under severe activation conditions involving large amounts of activating agents and/or high temperatures. Although effective for pore development, these conditions may increase chemical consumption, energy requirements and environmental constraints during the production process. In this study, the use of a low KOH impregnation ratio (0.1:1) and a moderate activation temperature (600 °C) resulted in estimated specific surface areas of 423-575 m^2.g^{-1} and methylene blue adsorption capacities of 380-492 mg.g^{-1}. These results suggest that combining biomass precursors can be an effective approach to improve adsorption properties while maintaining relatively moderate activation conditions.

Table 4. Langmuir, Freundlich and Pseudo-second-order parameters

			Langmuir			Freundlich			Pseudo -second - order		Weber-Morris		
Samples	Q_{exp} (mg.g^{-1})	Q_{max} (mg.g^{-1})	K_L	R^2_L	R_L	K_F	n	R^2_F	k_2	R^2_{PSO}	K_{id}	C	R^2_{WM}
CA-B	350	462	0.0562	0.8198	0.1290	67.8490	2.3641	0.7957	0.0025	0.9991	22.02	127.26	0.564
CA-C	304	353	0.1378	0.8983	0.0570	114.8039	3.8230	0.8777	0.0043	0.9987	41.42	74.17	0.488
CA-B20	314	477	0.0482	0.9717	0.1474	59.4002	2.2051	0.9458	0.0240	0.9991	21.87	136.14	0.527
CA-B50	315	492	0.0481	0.9635	0.1475	59.7912	2.1674	0.9364	0.0192	0.9985	42.10	74.55	0.479
CA-B80	364	380	0.4699	0.9976	0.0174	219.6013	6.8751	0.9990	0.0028	0.9985	26.13	153.32	0.553

$\boldsymbol{Q_{exp}}$ and $\boldsymbol{Q_{max}}$ are the experimental and maximum adsorption capacities, respectively (mg g^{-1}); $\boldsymbol{K_L}$ is the Langmuir constant; $\boldsymbol{R_L}$ is the Langmuir separation factor; $\boldsymbol{K_F}$ and $\boldsymbol{n}$ are the Freundlich constants; $\boldsymbol{k_2}$ is the pseudo-second-order rate constant; $\boldsymbol{k_{id}}$ is the intraparticle diffusion rate constant (mg.g^{-1}.min$^{-0,5}$); $\boldsymbol{C}$ is the intercept associated with the boundary-layer effect (mg.g^{-1}); and $\boldsymbol{R^2}$ is the coefficient of determination.

Table 5. Comparison of activation conditions, textural properties and adsorption performance of activated carbons derived from single and blended biomass feedstocks

Feedstock/Blend	Blend Ratio (w/w)	Activating Agent (Ratio, w/w)	Temperature (°C)	Performance Indicators	Reference
		Single Precursor			
Sugarcane bagasse		NaOH (0.1M) HCl (0.1M) Physical activation	900 900 400	S_{BET}: 458 m².g^{-1} S_{BET}: 20.4 m².g^{-1} S_{BET}: 25.7 m².g^{-1}	[52]
Coconut Shell		NaOH (4:1) H_3PO_4 (4:1) $ZnCl_2$ (4:1)	600°C	S_{BET}: 546 m².g^{-1} S_{BET}: 42 m².g^{-1} S_{BET}: 23 m².g^{-1}	[53]
Carob shel		0.1:1- 0.3:1	400	Adsorption capacity q_{max} Cd: 90.58 mg.g^{-1} q_{max} Co: 77.24 mg.g^{-1}	[54]
		Co-carbonization			
Willow wood with + homogenous biochar	1:1	$K_2C_2O_4$ (1:1)	800	S_{BET}: 1297-1409 m².g^{-1}	[55]
Licorice residue + Pistachio-nut shell		H_3PO_4, $ZnCl_2$ (0.5:1-2:1)	450-700	S_{BET}: 1013-1492 m².g^{-1}	[56]
Sewage sludge + Rice husk/ bamboo sawdust	1:1	Physical activation	400-700	S_{BET}: 0.68-10.71 m².g^{-1} higher metal immobilization and apparently lower biochar stability	[57]
Corn Stalk + Walnut Shell	1:1	H_3PO_4 (2.5:1)	500	Iodine number: 720.5 mg.g^{-1} Methylene blue number: 195.0 mg.g^{-1} S_{BET}: 1187 m².g^{-1}	[58]
Rice straw + Acid whey	0.05:1 0.15:1	Hydrothermal co - carbonization	200-300	Char yield increased by 20%	[59]
This Work: Sugarcane Bagase + Coconut shell	1:1 (50/50) 4:1(80/20) 1:4 (20/80)	KOH (0.1:1)	600	S_{est}: 423 m².g^{-1} S_{est}: 575 m².g^{-1} S_{est}: 452 m².g^{-1} MB Adsorption: 380-492 mg.g^{-1}	

S_{BET}: Specific surface area determined by the Brunauer-Emmett-Teller (BET) method**, S_{est}:** Estimated specific surface area by Nunes et al. method**, MB** = methylene blue**; q_{max}** = maximum adsorption capacity**; w/w** = weight ratio**.** The activating agent ratio refers to the mass ratio of activating agent to precursor.Conclusion

This study explores how co-carbonizing sugarcane bagasse and coconut shell affects the physicochemical properties and adsorption performance of KOH-activated carbons prepared under relatively mild conditions (600 °C, KOH/biomass ratio of 0.1:1). The blending ratio clearly influences the balance of synergistic effects between the two precursors: bagasse-rich blends promote microporosity and higher estimated specific surface area, while coconut-shell-rich blends increase oxygen-containing surface groups and alter the acid-base character of the surface. These complementary features affect methylene blue adsorption. Although CA-B80 developed the most porous structure, CA-B50 showed the highest adsorption capacity (492 $mg.g^{-1}$), suggesting that performance depends not only on pore development but also on the right balance between pore accessibility and surface chemistry. The adsorption kinetics were well fitted by the pseudo-second-order model, indicating that surface interactions played an important role. Overall, the results show that biomass blending can be an effective way to tune both pore structure and surface chemistry in activated carbons. More importantly, this performance was achieved with a much lower KOH impregnation ratio and a moderate activation temperature, which suggests that co-carbonization could help reduce chemical and energy demands while still delivering strong adsorption performance. These findings highlight the potential of two abundant tropical agro-industrial residues for producing activated carbons for water treatment.

Declarations

Funding

The authors received no financial support for the research, authorship, and/or publication of this article.

Conflict of Interest

The authors declare that they have no known competing financial or personal relationships that could have appeared to influence the work reported in this paper.

References

[1] Jjagwe J, Olupot PW, Menya E, et al. Synthesis and Application of Granular Activated Carbon from Biomass Waste Materials for Water Treatment: A Review. *J Bioresour Bioprod*. 2021; 6(4): 292-322.

[2] Pereira L, Castillo V, Calero M, et al. Promoting the circular economy: Valorization of a residue from industrial char to activated carbon with potential environmental applications as adsorbents. *J Environ Manage*. 2024; 356: 120753.

[3] Luo L, Lan Y, Zhang Q, et al. A review on biomass-derived activated carbon as electrode materials for energy storage supercapacitors. *J Energy Storage*. 2022; 55: 105839.

[4] Daud W. Comparison on pore development of activated carbon produced from palm shell and coconut shell. Bioresour Technol. 2004; 93(1): 63-69.

[5] Joshi S, K.c B. Synthesis and Characterization of Sugarcane Bagasse Based Activated Carbon: Effect of Impregnation Ratio of ZnCl2. *J Nepal Chem Soc*. 2020; 41(1): 74-79.

[6] A P Ramirez, S Giraldo, M Ulloa, et al. Production and characterization of activated carbon from wood wastes. *OP Conf Ser J Phys Conf Ser* 935 2017 012012. 2017.

[7] Lin B, Zhou J, Qin Q, et al. Physicochemical characteristics of biomass-coal blend char: The role of co-pyrolysis synergy. *Energy Sci Eng.* 2021; 9.

[8] Wang A-Y, Sun K, Wu L, et al. Co-carbonization of biomass and oily sludge to prepare sulfamethoxazole super-adsorbent materials. *Sci Total Environ*. 2020; 698: 134238.

[9] Koido K, Endo K, Morimoto H, et al. Synergistic Effects in Co-Gasification of Willow and Cedar Blended Char in CO2 Media. *Energies*. 2024; 17: 4122.

[10] Bambalaza SE, Xakalashe BS, Coetsee Y, et al. Co-Carbonization of Discard Coal with Waste Polyethylene Terephthalate towards the Preparation of Metallurgical Coke. *Materials*. 2023; 16(7): 2782.

[11] Mulyani S, Hayati W, Silvia M, et al. MANUFACTURING COCONUT SHELL CHARCOAL BRICKETS AND SUGAR CANE AS ALTERNATIVE FUEL. *J Ris Fis Edukasi Dan Sains.* 2024; 11: 53-64.

[12] Gusiatin MZ. Advantages of Co-Pyrolysis of Sewage Sludge with Agricultural and Forestry Waste. *Energies*. 2024; 17(22): 5736.

[13] Mohamed BA, Li LY. Biofuel production by co-pyrolysis of sewage sludge and other materials: a review. *Environ Chem Lett.* 2023; 21(1): 153-182.

[14] Zhang H, Qiao Y, Jin R, et al. Synergistic effects of biochar from the co-pyrolysis of lignocellulosic biomass and typical biomasses: mechanism of action and key parameters. *Bioresour Technol.* 2026; 458: 135117.

[15] Guclu C, Alper K, Erdem M, et al. Activated carbons from co-carbonization of waste truck tires and spent tea leaves. *Sustain Chem Pharm.* 2021; 21: 100410.

[16] Liang Q, Liu Y, Chen M, et al. Optimized preparation of activated carbon from coconut shell and municipal sludge. *Mater Chem Phys.* 2020; 241: 122327.

[17] Lin F, Wu J, Zhang Z, et al. Sustainable nitrogen-doped biochar derived from dual agricultural wastes for water treatment. *J Water Process Eng.* 2026; 91: 110469.

[18] Boehm HP. Chemical Identification of Surface Groups. In: Eley DD, Pines H, Weisz PB, editors. *Adv Catal* [Internet]. Academic Press; 1966 [cited 2026 June 15]. p. 179-274. Available from: https: //www. sciencedirect.com/ science/ article/ pii/ S0360056408603545.

[19] Oickle A, Goertzen S, Hopper K, et al. Standardization of the Boehm titration: Part II. Method of agitation, effect of filtering and dilute titrant. *Carbon*. 2010; 48: 3313-3322.

[20] Goertzen SL, Thériault KD, Oickle AM, et al. Standardization of the Boehm titration. Part I. CO2 expulsion and endpoint determination. *Carbon*. 2010; 48(4): 1252-1261.

[21] ASTM International. Standard Test Method for Determination of Iodine Number of Activated Carbon. West Conshohocken, PA, USA; 2006. Report No.: *ASTM D4607-94*.

[22] European Chemical Industry Council (CEFIC). Test Methods for Activated Carbon. Brussels, Belgium; 1986.

[23] Cleiton A. Nunes e Mário C. Guerreiro. Estimation of surface area and pore volume of activated carbons by methylene blue and iodine numbers [Internet]. 2011 [cited 2026 June 9]. Available from: https: //www. researchgate.net/ publication/ 255748062_Estimation_of_surface_area_and_pore_volume_of_activated_carbons_by_methylene_blue_and_iodine_numbers.

[24] Xie M, Cheng J, Xu L, et al. Preparation of Activated Carbon from Co-Pyrolysis Activation of Fly Ash and Biomass. *Energies.* 2022; 15(18): 6636.

[25] Zubrik A, Matik M, Hredzák S, et al. Preparation of chemically activated carbon from waste biomass by single-stage and two-stage pyrolysis. *J Clean Prod*. 2017; 143: 643-653.

[26] Bouassa Mougnala S, Mve Mfoumou C, Mbouiti B, et al. Elimination, Kinetics and Thermodynamics of Fe(II) Ions by Adsorption in Static and Dynamic Conditions on Activated Carbons in Aqueous Media. *J Geosci Environ Prot.* 2024; 12: 181-203.

[27] Anatole KIFUANI KIA MAYEKO. Adsorption de la quinine bichlorhydrate sur un charbon actif peu coûteux à base de la Bagasse de canne à sucre imprégnée de l'acide phosphorique. 2012.

[28] Yuming Wen et Al, 2021. Synergistic effect of the co-pyrolysis of cardboard and polyethylene: A kinetic and thermodynamic study. 2021.

[29] Yin H, Huang X, Song X, et al. Co-pyrolysis of de-alkalized lignin and coconut shell via TG/DTG-FTIR and machine learning methods: pyrolysis characteristics, gas products, and thermo-kinetics. *Fuel*. 2022; 329: 125517.

[30] Dong X, Wang Z, Zhang J, et al. Synthesis and characteristics of carbon-based synfuel from biomass and coal powder by synergistic co-carbonization technology. *Renew Energy*. 2024; 227: 120458.

[31] Vuppaladadiyam AK, Vuppaladadiyam SSV, Sikarwar VS, et al. A critical review on biomass pyrolysis: Reaction mechanisms, process modeling and potential challenges. *J Energy Inst*. 2023; 108: 101236.

[32] Brebu M, Vasile C. Thermal degradation of lignin - A Review. *Cellul Chem Technol*. 2010; 44: 353-363.

[33] Zakaria R, Jamalluddin NA, Abu Bakar MZ. Effect of impregnation ratio and activation temperature on the yield and adsorption performance of mangrove based activated carbon for methylene blue removal. *Results Mater*. 2021; 10: 100183.

[34] Neolaka YAB, Riwu AAP, Aigbe UO, et al. Potential of activated carbon from various sources as a low-cost adsorbent to remove heavy metals and synthetic dyes. *Results Chem*. 2023; 5: 100711.

[35] Raposo F, De La Rubia MA, Borja R. Methylene blue number as useful indicator to evaluate the adsorptive capacity of granular activated carbon in batch mode: Influence of adsorbate/adsorbent mass ratio and particle size. *J Hazard Mater*. 2009; 165(1-3): 291-299.

[36] Yang J, Han S. Kinetics and equilibrium study for the adsorption of lysine on activated carbon derived from coconut shell. *DESALINATION WATER Treat*. 2018; 120: 261-271.

[37] Wang X, Li D, Li W, et al. Optimization of Mesoporous Activated Carbon from Coconut Shells by Chemical Activation with Phosphoric Acid. *BioResources*. 2013; 8(4): 6184-6195.

[38] Altwala A, Mokaya R. Modulating the porosity of activated carbons via pre-mixed precursors for simultaneously enhanced gravimetric and volumetric methane uptake. *J Mater Chem A*. 2022; 10(26): 13744-13757.

[39] Rodríguez-Reinoso F, Molina-Sabio M. Activated carbons from lignocellulosic materials by chemical and/or physical activation: an overview. *Carbon*. 1992; 30(7): 1111-1118.

[40] Lillo-Ródenas MA, Cazorla-Amorós D, Linares-Solano A. Understanding chemical reactions between carbons and NaOH and KOH: an insight into the chemical activation mechanism. *Carbon*. 2003; 41(2): 267-275.

[41] Contescu A, Contescu C, Putyera K, et al. Surface acidity of carbons characterized by their continuous pK distribution and Boehm titration. *Carbon*. 1997; 35(1): 83-94.

[42] Yang H, Yan R, Chen H, et al. Characteristics of hemicellulose, cellulose and lignin pyrolysis. *Fuel*. 2007; 86(12): 1781-1788.

[43] Lozano-Castelló D, Lillo-Ródenas MA, Cazorla-Amorós D, et al. Preparation of activated carbons from Spanish anthracite: I. Activation by KOH. *Carbon*. 2001; 39(5): 741-749.

[44] Montes-Morán MA, Suárez D, Menéndez JA, et al. On the nature of basic sites on carbon surfaces: an overview. *Carbon*. 2004; 42(7): 1219-1225.

[45] Gutierrez-Martinez J, Martinez-Vargas D, Vences E, et al. Point of zero charge, isoelectric point, and potential of zero charge on activated carbons: A comprehensive interpretation about their interrelation. *Curr Opin Solid State Mater Sci*. 2026; 40: 101247.

[46] Ho YS, McKay G. Pseudo-second order model for sorption processes. *Process Biochem*. 1999; 34(5): 451-465.

[47] Giles CH, MacEwan TH, Nakhwa SN, et al. Studies in adsorption. Part XI. A system of classification of solution adsorption isotherms, and its use in diagnosis of adsorption mechanisms and in measurement of specific surface areas of solids. *J Chem Soc Resumed*. 1960; (0): 3973-3993.

[48] Foo KY, Hameed BH. Insights into the modeling of adsorption isotherm systems. *Chem Eng J*. 2010; 156(1): 2-10.

[49] Jawad AH, Abdulhameed AS, Bahrudin NN, et al. Microporous activated carbon developed from KOH activated biomass waste: surface mechanistic study of methylene blue dye adsorption. *Water Sci Technol*. 2021; 84(8): 1858-1872.

[50] Pelekani C, Snoeyink VL. Competitive adsorption in natural water: role of activated carbon pore size. *Water Res*. 1999; 33(5): 1209-1219.

[51] Altenor S, Carene B, Emmanuel E, et al. Adsorption studies of methylene blue and phenol onto vetiver roots activated carbon prepared by chemical activation. *J Hazard Mater*. 2009; 165(1): 1029-1039.

[52] Nur Layli Amanah, Alsello Diveni Manuputty, Fadila Arum Ramadhani, et al. Adsorption behavior of sugarcane bagasse-derived activated carbon as a copper removal. *Indonesian Journal of Applied Physics* (IJAP) Vol. 15 No. 1 page 98. 2025.

[53] Sujiono EH, Zabrian D, Zurnansyah, et al. Fabrication and characterization of coconut shell activated carbon using variation chemical activation for wastewater treatment application. *Results Chem*. 2022; 4: 100291.

[54] Farnane M, Machrouhi A, Elhalil A, et al. Process optimization of potassium hydroxide activated carbon from carob shell biomass and heavy metals removal ability using Box-Behnken design. *Desalination Water Treat*. 2018; 133: 153-166.

[55] Cheng X, Jiang Y, Sun K, et al. Syngenetic effects in co-activation of willow wood with homogenous biochar facilitate pore generation in activation. *J Anal Appl Pyrolysis*. 2024; 182: 106717.

[56] Kaghazchi T, Asasian N, Soleimani M. Licorice residue and Pistachio-nut shell mixture: A promising precursor for activated carbon. *J Ind Eng Chem*. 2010; 16: 368-374.

[57] Zhang J, Jin J, Wang M, et al. Co-pyrolysis of sewage sludge and rice husk/ bamboo sawdust for biochar with high aromaticity and low metal mobility. *Environ Res*. 2020; 191: 110034.

[58] Kang C, Shang D, Yang T, et al. Preparation of Corn Stalk-walnut Shell Mix-based Activated Carbon and Its Adsorption of Malachite Green. *Chem Res Chin Univ*. 2018; 34(6): 1014-1019.

[59] Zhao Y, Lu T, Xu G, et al. Hydrothermal co-carbonization of rice straw and acid whey for enhanced hydrochar properties and nutrient recovery. *Green Energy Resour*. 2024; 2(2): 100077.